Supporting Information

Structural Phase Transition due to Flexible Supramolecule of (4-Cyanomethylanilinium)([18]crown-6) in $[Ni(dmit)_2]^-$ Crystal

Qiong Ye, Tomoyuki Akutagawa, Heng-Yun Ye, Tian Hang, Jia-Zhen Ge, Ren-Gen Xiong, Takemitsu Kikuchi, Shin-ichiro Noro, and Takayoshi Nakamura

Full list of all authors in Ref. 17

Frisch, M. J.; Trucks, G. W.; Schlegel, H. B.; Scuseria, G. E.; Robb, M. A.; Cheeseman, J. R.; Zakrzewski, V. G.; Montgomery, J. A., Jr.; Stratmann, R. E.; Burant, J. C.; Dapprich, S.; Millam, J. M.; Daniels, A. D.; Kudin, K. N.; Strain, M. C.; Farkas, O.; Tomasi, J.; Barone, V.; Cossi, M.; Cammi, R.; Mennucci, B.; Pomelli, C.; Adamo, C.; Clifford, S.; Ochterski, J.; Petersson, G. A.; Ayala, P. Y.; Cui, Q.; Morokuma, K.; Malick, D. K.; Rabuck, A. D.; Raghavachari, K.; Foresman, J. B.;. Cioslowski, J.; Ortiz, J. V.; Baboul, A. G.; Stefanov, B. B.; Liu, G.; Liashenko, A.; Piskorz, P.; Komaromi, I.; Gomperts, R.; Martin, R. L.; Fox, D. J.; Keith, T.; Al-Laham, M. A.; Peng, C. Y.; Nanayakkara, A.; Gonzalez, C.; Challacombe, M.; Gill, P. M. W.; Johnson, B.; Chen, W.; Wong, M. W.; Andres, J. L.; Gonzalez, C.; Head-Gordon, M.; Replogle, E. S.; Pople, J. A. *GAUSSIAN 98*; Gaussian, Inc.: Pittsburgh, PA, 1998.

1. Optical Properties

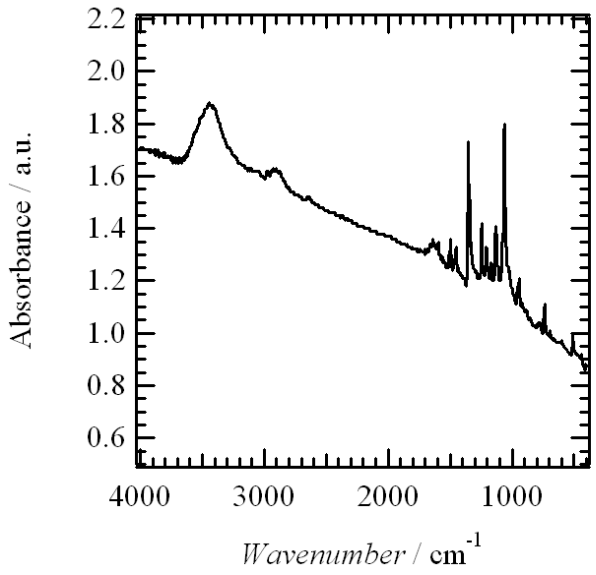

Figure S1. IR spectrum in KBr pellet.

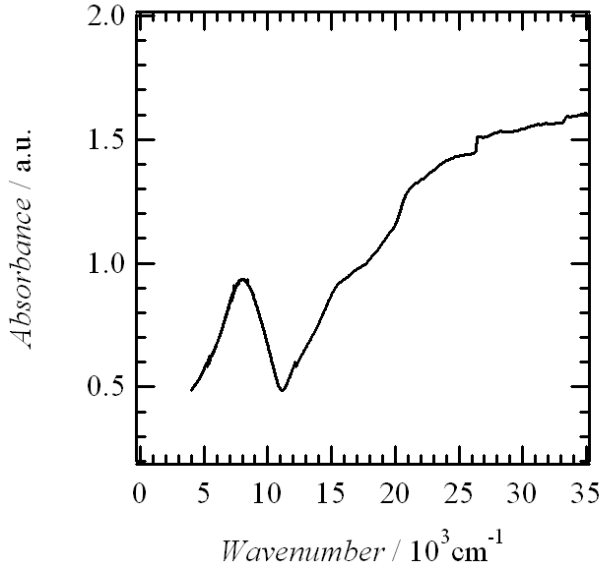

Figure S2. UV-vis-NIR spectrum in KBr pellet.

2. X-ray Crystal Structural Analysis

All measurements were made on a Rigaku RAXIS RAPID imaging plate area detector with graphite monochromated Mo-Ka radiation. Indexing was performed from 3 oscillations that were exposed for 1050 seconds. The crystal-to-detector distance was 127.40 mm.

The data were collected at a maximum 2θ value of 55.0°. A sweep of data was done using ω scans from 130.0 to 190.0° in 3.0o step, at χ=45.0° and φ = 30.0°. The exposure rate was 402.0 [sec./°]. A second sweep was performed using w scans from 0.0 to 159.0o in 3.0o step, at χ=45.0o and φ = 210.0o. The exposure rate was 402.0 [sec./o]. Another sweep was performed using w scans from 0.0 to 159.0° in 3.0° step, at χ=0.0° and φ = 210.0°. The exposure rate was 402.0 [sec./°]. The crystal-to-detector distance was 127.40 mm. Readout was performed in the 0.100 mm pixel mode. An empirical absorption correction was applied which resulted in transmission factors ranging from 0.60 to 1.00. The data were corrected for Lorentz and polarization effects.

The structure was solved by direct methods and expanded using Fourier techniques. The non-hydrogen atoms were refined anisotropically. Hydrogen atoms were refined using the riding model. The final cycle of full-matrix least-squares refinement on F^2 was based on observed reflections and variable parameters and converged (largest parameter shift was 0.00 times its esd) with unweighted and weighted agreement factors of $R_1 = \Sigma||Fo|-|Fc||/\Sigma|Fo|$ and $wR_2 = [\Sigma(\omega(Fo^2-Fc^2)^2)/ \Sigma\omega(Fo^2)^2]^{1/2}$. A Robust-resistant weighting scheme was used. Plots of $\Sigma\omega(|Fo|-|Fc|)^2$ versus |Fo|, reflection order in data collection, sin q/l and various classes of indices showed no unusual trends.

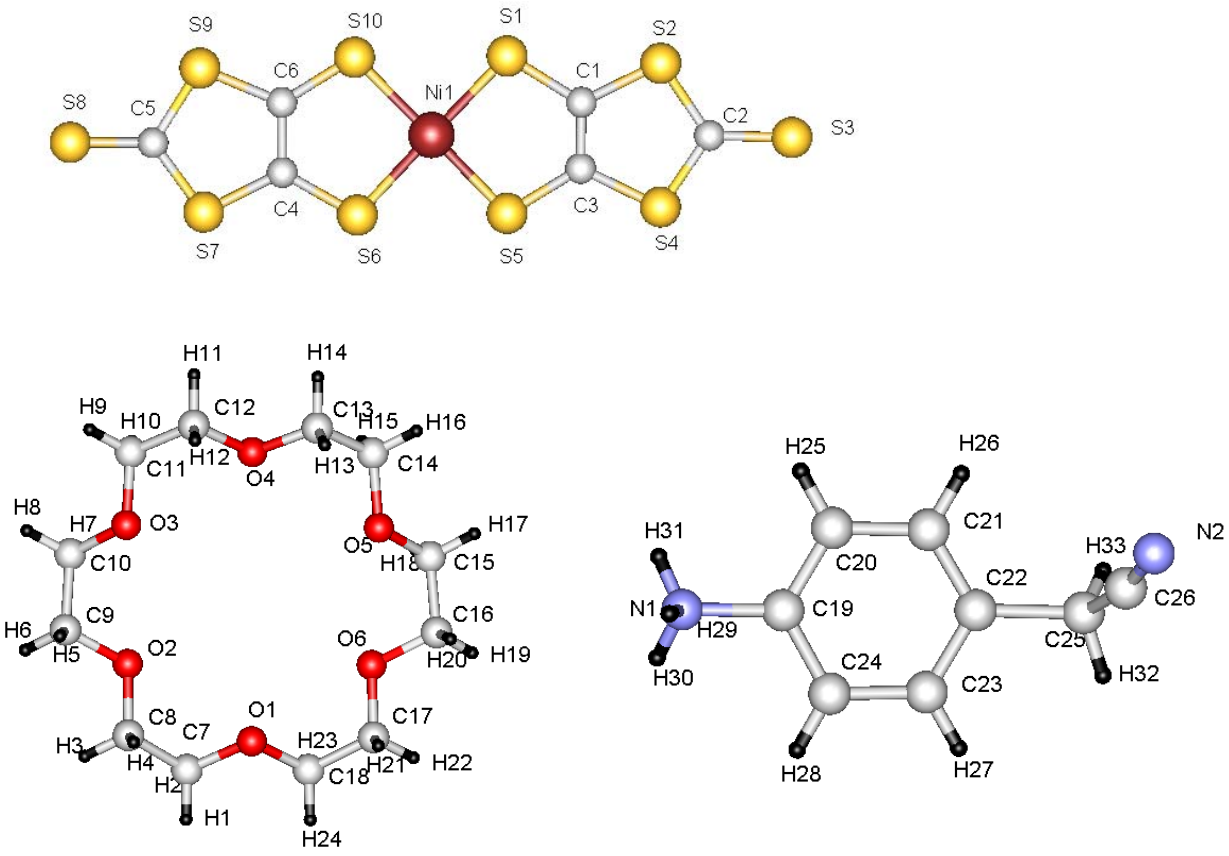

Figure S3. Atomic numbering scheme of crystal **1** at 300 K.

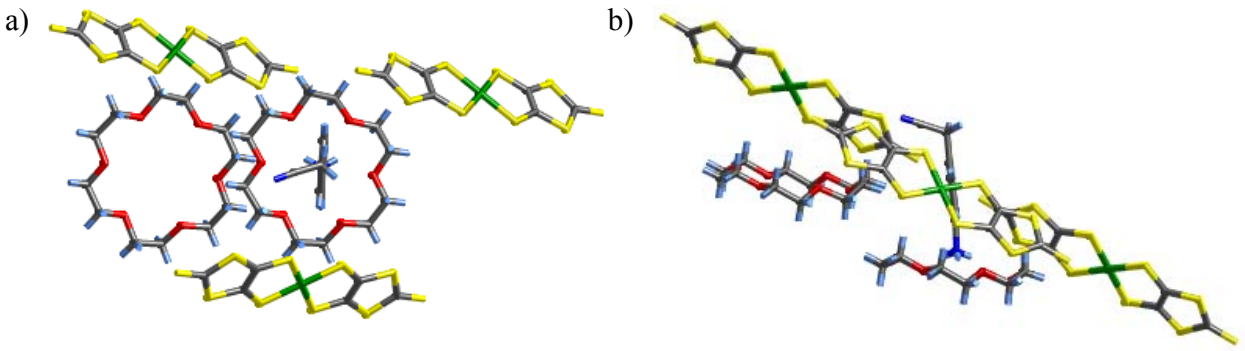

Figure S4. Model structure of $(CMAni^{+})([18]crown\text{-}6)_2[Ni(dmit)_2]_3$ for the calculation of phenyl-ring rotation along the C - N axis viewed along the a) C - N axis and b) along the π-plane of phenyl-ring.

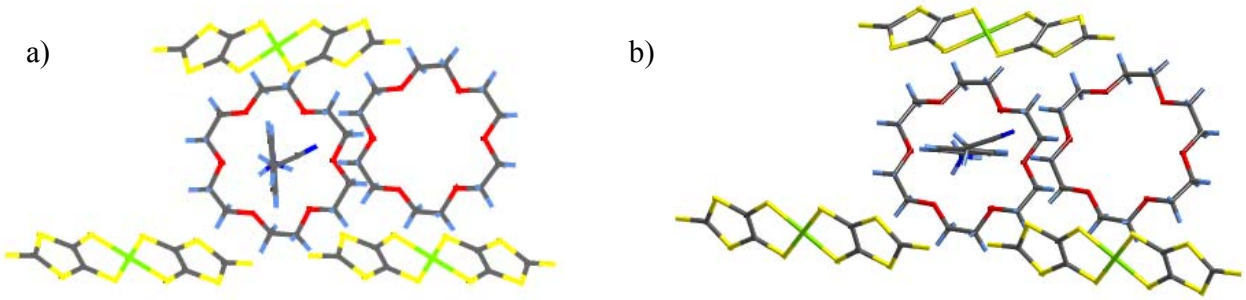

Figure S5. Model structure of $(CMAni^{+})([18]crown\text{-}6)_2[Ni(dmit)_2]_3$. The rotation angle of a) $\phi_1 = 0°$ and b) $\phi_1 = 90°$.

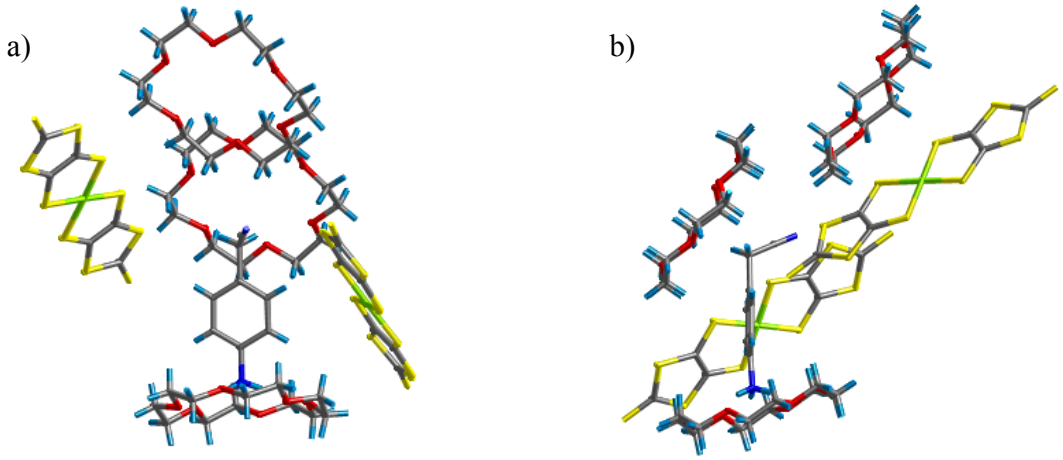

Figure S6. Model structure of $(CMAni^{+})([18]crown\text{-}6)_3[Ni(dmit)_2]_2$ for the calculation of cyanomethy rotation along the C - C axis viewed a) normal to the π-plane of phenyl-ring and b) parallel to the π-plane of phenyl-ring.

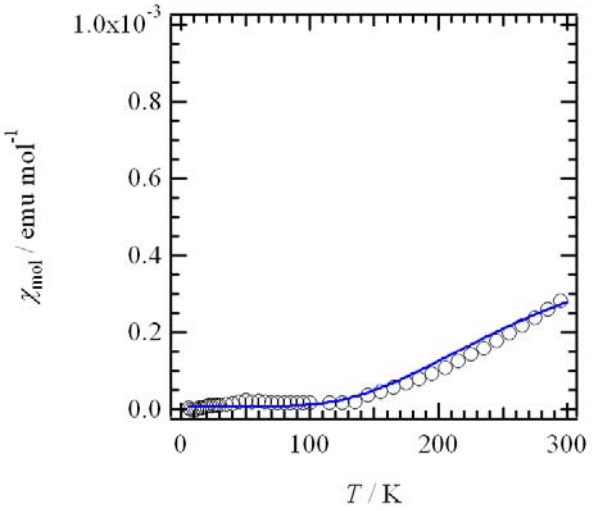

Figure S7. Temperature dependent magnetic susceptibility. The blue-line was a fit by dimer model.